Neural Network Models for the Half-Cell Potential of Reinforced Slabs with Magnesium Sacrificial Anodes Subjected to Chloride Ingress

Yogesh Iyer Murthy[1*] iD

1. Assistant Professor, Department of Civil Engineering, Jaypee University of Engineering and Technology, Guna, Madhya Pradesh, India
Corresponding author: *yogesh.murthy@juet.ac.in*

https://doi.org/10.22115/SCCE.2023.347658.1470

ARTICLE INFO	ABSTRACT
	This study develops prediction models using Artificial Neural Network (ANN) to describe the long term performance of reinforcements in concrete slabs containing pure Magnesium anodes and subjected to chloride ingress. Ten reinforced concrete slabs of dimensions 1000 mm x 1000 mm x 100 mm were cast. Five slabs were cast with 3.5% NaCl by weight of cement, and five more were cast without NaCl. The distance of the point under consideration from the anode in the x and y axes, temperature, relative humidity (RH), and age of concrete in days were considered input parameters, while the half-cell potential (HCP) values with reference to the Standard Calomel Electrode (SCE) were considered output. Experimental values consisting of 80 HCP values per slab per day were collected for 270 days and were averaged for both cases to generate the prediction model. Various learning heuristics used in supervised learning in feedforward ANN was used (viz. RB, OSS, SCG, GDA, CGP, CGF, GDX, and LM). A two-layer feed-forward network with 10 sigmoid hidden neurons and trained linear output neurons was employed in this work. The network architecture [5-10-1] and 10 neurons in the hidden layer were used for all the prediction models. Out of all the training algorithms used, the overall performance was best with LM in all stages of modelling (>96%). To conclude, the prediction of HCP values through the neural network models based on the available experimental data set was excellent.

1. Introduction

Reinforced concrete (RC) is the most common material used in the construction industry [1]. While the concrete provides high compressive strength, the steel reinforcement embedded in the concrete provides high tensile and flexural strength [2]. Thus, the composite material, namely RC, is versatile as far as strength characteristics are concerned. But the presence of free chloride ions, carbonates, sulfates, and other ionic materials is reported to be detrimental to the steel reinforcement as they initiate corrosion [3]. This affects the structural performance of steel. Among these ions, the ingress of chloride is the most detrimental factor affecting the structural performance of RC structures, especially those exposed to the marine atmosphere [4]. Hence, the development of various novel techniques to mitigate corrosion is an active area of research in the design of offshore structures. Several techniques to prevent corrosion are reported by researchers worldwide. These include the use of stainless steel and galvanized steel [5], corrosion-resistant steel reinforcements [6], the use of corrosion inhibitors [7–11], paints [12], epoxy coatings [13], laminates and reinforced plastics [14], and the use of sacrificial anodes [15–22]. For marine structures exposed to free chloride ions, the use of sacrificial anodes, also known as the cathodic protection technique, provides an effective and practically viable solution [21]. This method effectively stops the corrosion process, shifting the potential of reinforcement to a range of minimum possibility of corrosion.

The cathodic protection technique involves the formation of an electrochemical cell in the concrete structure [23]. Metals, such as Magnesium (Mg) and its alloys, Aluminum and Zinc, with high electronegative potential are used for this purpose. They are connected with the reinforcement of the structure, which is rendered cathode due to its lower negative electrochemical potential. The pore solution that is available in the concrete acts as an electrolyte [24]. The metals, being anodes, interact with the ions and, in turn, are rapidly consumed, hence the name sacrificial anode (Fig 1.)
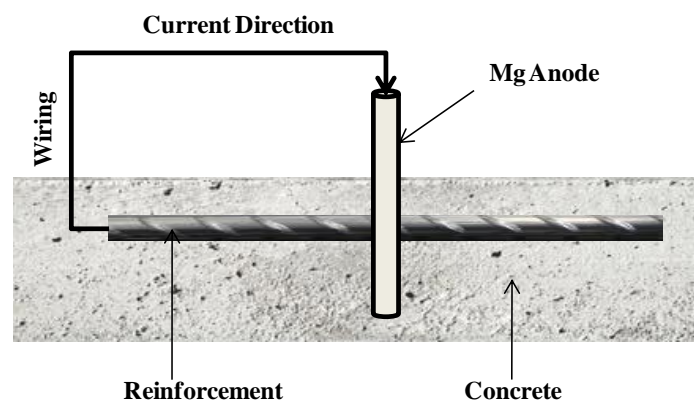

Fig. 1. Schematic of cathodic protection of reinforcement.

Mg and its alloys are the most commonly used sacrificial anodes since they possess a high electronegative potential (i.e., 2.34 V). Significant literature on the experimental investigations involving corrosion mitigation using Mg alloys as sacrificial anodes is available [25–27]. But in general, such investigations are conducted over a relatively long period of time to arrive at

conclusions. For example, the experimental work of Parthiban et al. [14] was carried out for 42 months on the Mg alloy anodes and reported a decrease in chloride content with time. Due to the inherent complexities involved with prolonged experimentation, many researchers have resorted to proposing models to predict corrosion of reinforcements [28–31]. These models are bound to stipulated conditions, and their applications are limited by assumptions such as uniform oxygen concentration distribution and rapid formation of the hydroxide film on steel [32]. A satisfactory agreement of these models with experimental data is reported for the given corrosion environment in the system. However, to the author's knowledge, long-term predictions using any of these models have not been reported. Hence, a measurable model is required to be developed to predict and analyse the corrosion state of reinforcement in concrete. The simplest measure of corrosion in reinforcement is a measurement of HCP [33]. These values can later be compared with the stipulations laid out by international standards, such as, ASTM C876 [34]. The main goal of the current research is to assess and analyze the performance of several Artificial Neural Network (ANN) strategies for foretelling the corrosion of embedded steel using HCP data. Secondly, to provide an ideal ANN model that based on HCP values, can properly forecast the corrosion of embedded steel.

2. Research significance

This study proposes a data-driven approach based on ANN for the prediction of HCP values and considers the major environmental factors affecting corrosion of reinforcements. These values of HCP indicate the probability of corrosion based on international standards. Also, unlike most of the prediction models developed, this work predicts the HCP values based on the prevailing atmospheric conditions and hence is not bound by assumptions and stipulations. The study involves the use of an experimental data set taken for 270 days using ten different training algorithms. The performance and application of the proposed ANN model are further verified for a standard slab and are found to be in excellent agreement with experimental results; a high R-value is reported. Thus, the models presented in this work can be conveniently used to predict the probability of corrosion, given the value of HCP.

3. Materials and experimental setup

Ten reinforced concrete slabs of dimensions 1000 mm x 1000 mm x 100 mm were cast. A steel reinforcement mat of 10 mm diameter with a clear cover of 25 mm from all sides and a centre-to-centre spacing of 190 mm, as shown in Fig. 2, was placed in the formwork. The surface area of the steel reinforcement mat was found to be 1.884 m^2. The reinforcements were treated with pickling solution to remove existing corrosion sites, if any. Pure Mg anodes of 22 mm diameter and 250 mm long were centrally placed and cast monolithically to complete the electrochemical cell. Insulated copper wires were soldered at the ends of the reinforcements and then covered with epoxy. These wires were necessary for measuring the HCP values using the Standard Calomel Electrode (SCE).

Nominal concrete of ratios 1:1.5:3 and water to cement ratio of 0.45 was used. The first set of five slabs (Slab #1) were cast with 3.5% NaCl by weight of cement, and the second set of five

slabs (Slabs #2) were cast without NaCl. These slabs were constructed using portable water with specifications shown in Table 1. The casting of both slabs was done on the same day to maintain similar casting conditions. The specifications provided by IS: 456-2000 [35] and IS: 10262-2019 [36] were used in the selection of ingredients, design and curing. The experimental input data included monitoring of temperature, RH, HCP values, distance from the anode, and the age of the concrete in days.
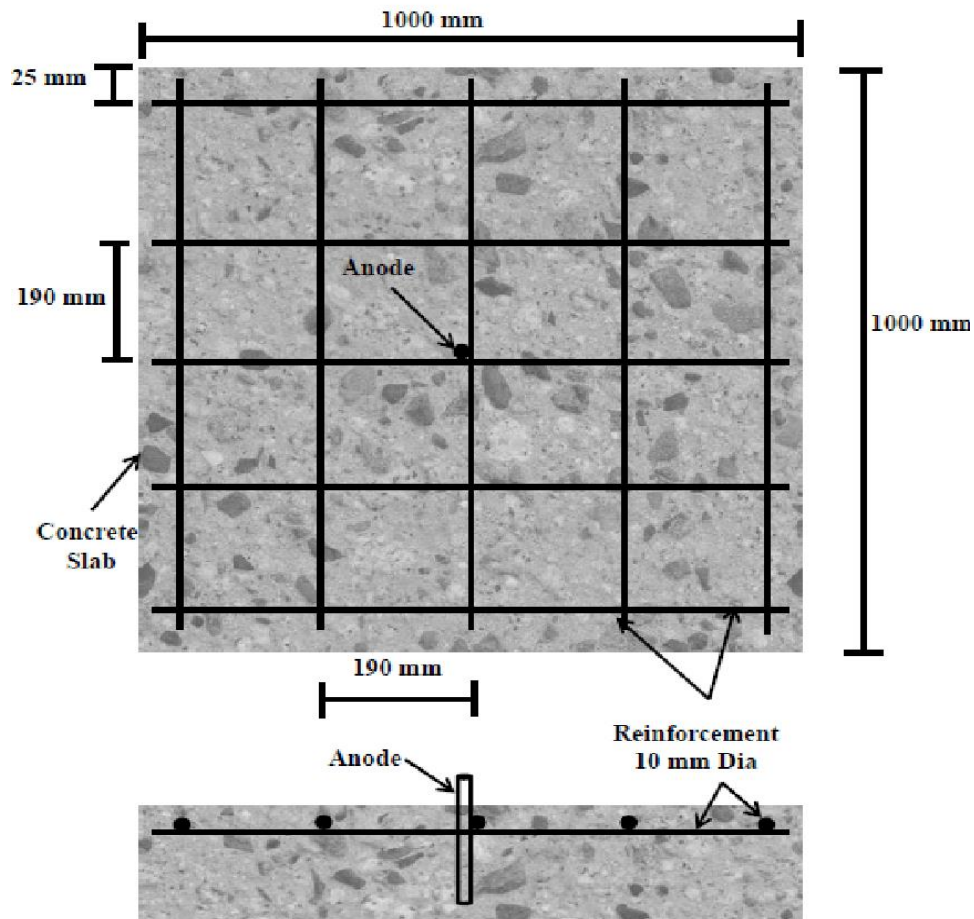

Fig. 2. Schematic of the slab with anode and reinforcement details.

Table 1
Portable water characteristics.

S No.	Parameter	Value
1	Chloride	168mg/l
2	pH	7.6
3	Fluoride	0.4mg/l
4	Dissolved Oxygen	10.15mg/l
5	Chemical Oxygen Demand	0
6	Biological Oxygen Demand	0
7	Free Residual Chlorine	0.1mg/l

OPC 53 grade provided by UltraTech cement, confirming IS 12269-2013 [37] was used in this work. The physical properties of cement used in the construction of slabs are presented in Table. 2.

Table 2
Physical Properties of OPC (53 grade).

Fineness (%)	Le Chatelier Soundness (mm)	Specific Gravity	Consistency (mins.)	Setting Time (mins.)		Compressive strength (MPa)		
				IST	FST	3 Day	7 day	28 days
2.10	8	3.15	30	100	250	28	40	57

The chemical properties following IS 12269-2013 [37] were also evaluated and are presented in Table 3.

Table 3
Chemical Properties of OPC (53 grade) in %.

Loss on ignition	CaO	SiO2	Al2O3	Fe2O3	MgO	K_2O	Na_2O
3	66.72	18.93	4.57	4.90	0.83	0.45	0.12

River sand provided by Rajalaxmi Crusher and Sand Plant, Awan, India, conforming to grading zone II of IS: 383-2016 [38] was used in this work, with particle size distribution as shown in Fig.3.
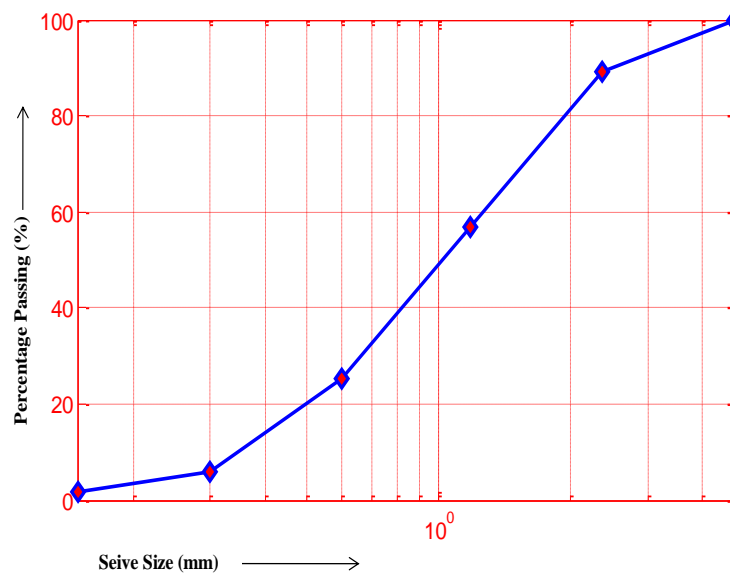

Fig. 3. Particle size distribution of sand.

Fig. 4 shows the relevant points where measurement of HCP values was done in both the slabs.
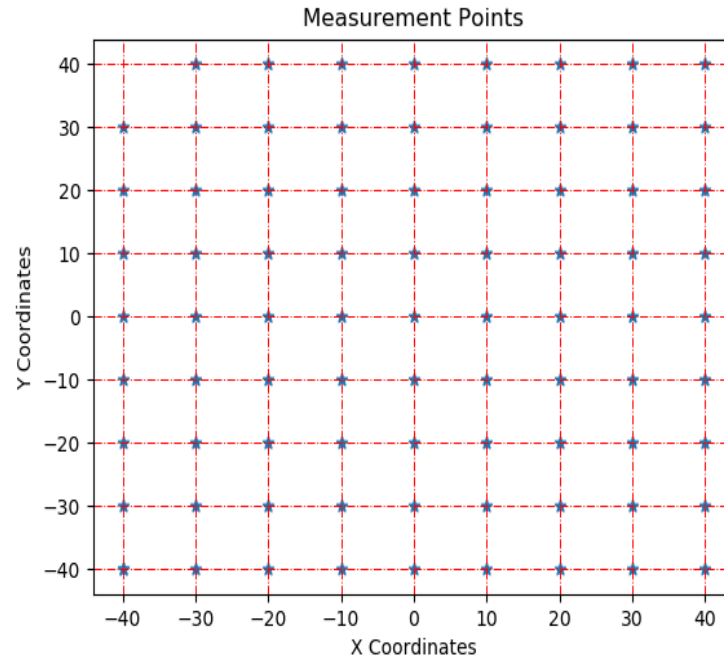
Fig.4. Location of points where HCP readings were taken.

4. ANN

John McCarthy coined the term "Artificial Intelligence" in 1956 at a conference in Dartmouth. Artificial's mimicking of human behavior. The research of developing a computer system that can replicate human intellect is known as artificial intelligence. Warren McCulloch and Pitts [39] published the first mathematical model based on biological neurons in 1943, which sparked the development of the first artificial neuron.

An advanced form of machine learning algorithm known as ANN resembles the neurons in the human brain. In general, many neurons join together to create an ANN, which functions as the basis for the execution of a function in line with its mission. Engineering disciplines as diverse as ocean engineering, hydraulics, and geotechnical engineering have all employed ANN for nonlinear modeling. "Input signals" are the signals or samples that depict the values conjectured by the variables of a certain application. The input signals are often adjusted in order to increase the computational efficiency of learning algorithms. A weight, known as a synaptic weight, is assigned to each input variable, allowing the significance of each one to the operation of the neuron to be measured [40].

The output of the linear aggregator should have the proper threshold to serve as a trigger value for the neuron output, and this threshold is defined by the variable known as the bias (activation threshold). By virtue of its functional image, AF serves the objective of restricting neuron output within an appropriate range of values. The final value that a neuron generates in response to a particular collection of input signals is known as the output signal. Moreover, it may act as an input for additional, sequentially linked neurons [40]. The ANN architecture used in this model is 5-10-1 and is shown in Fig. 5.
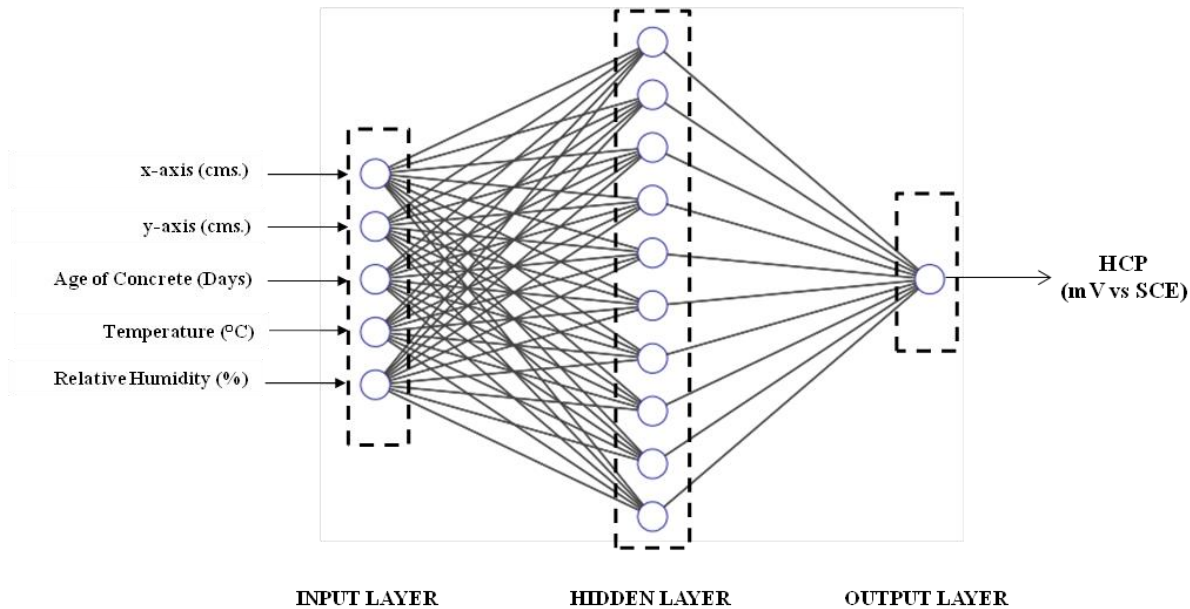
Fig. 5. Neural network architecture for proposed model.

The task of gathering data (information), signals, and features from the external domain falls to the input layer. Neurons in the hidden layer are in charge of finding patterns associated with the system or process being researched. These layers handle much of the network's internal operations. The four categories of single-layer feed-forward networks, multilayer feed-forward networks, recurrent networks (feedback architecture), and mesh networks may be used to classify the fundamental ANN designs. The term "epoch" in machine learning (ML) refers to all of the algorithm's runs throughout the whole training dataset [41–43].

Table 4
Acronym of various algorithms.

S. No	Acronym	Algorithm
1	RB	Resilient Backpropagation
2	SCG	Scaled Conjugate Gradient
3	CGF	Fletcher-Powell Conjugate Gradient
4	CGP	Polak-Ribiére Conjugate Gradient
5	OSS	One-Step Secant
6	GDX	Variable Learning Rate Backpropagation
7	GDA	Gaussian discriminant analysis
8	LM	Levenberg-Marquardt

The Neural Network Toolbox in MATLAB R2014a was employed to develop an ANN model for predicting the HCP values based on the input parameters, namely, distance in x, distance in y, age of concrete, temperature and relative humidity. The descriptive statistics of these parameters are presented in Table 5. The division of data into training, validation, and testing was random. 70 % of the data was used for training while 15 % each of the remaining data was used for testing and

validation respectively. Feedforward backpropagation was used to obtain the optimum model, as it decreases the error between model output and target output by reducing the mean square error (MSE) for a given training set. The sigmoid function is selected as an activation function as it allows for non-linear decision boundaries. A training algorithm identifies a decision function which changes the network's weights. There are several training algorithm variants. Some of them are listed in Table 4 and were covered in the scope of this research. It is difficult to predict which training algorithm will yield the best results [41].The algorithms were used as training functions to update the weights and bias value, and their performance was compared. The optimum number of neurons in the hidden layers based on R^2 value was found to be 10. A brief over various training algorithms used is presented here.

Table 5
Descriptive statistics of the parameters.

S. No.	Parameter	Input parameters					Output parameter
		Distance in x	Distance in y	Age of Concrete	Temperature	RH	HCP
	Unit	cm.	cm.	Days	°C	%	(mV vs SCE)
1	Mean	-	-	150	30.5	48	-670
2	Median	-	-	150	31.5	37.5	-660
3	Range						
	Maximum	40	40	0	36	13	-512
	Minimum	-40	-40	270	14	81	-752

From (1) through (10), a vector of x_k stands for the current weights and biases, g_k for the current gradient of the error with respect to the weight vector, a_k for the learning rate (or step size), x_{k+1} for a new weight vector, and k for the number of iterations the techniques have undergone.

4.1. Resilient backpropagation

RP is a heuristic learning method that improves convergence time by employing just the sign of the derivative of the error function for the weight update, as demonstrated in (1). RP decreases the number of learning steps and other adaptation factors, according to GDA's and it easily computes local learning schemes [44].

$$\Delta x_k = -sign \frac{\Delta E_k}{\Delta x_k} \Delta k \tag{1}$$

Where:

Δx_k = changes of current weights vector;

ΔE_k = error function E at k

Δk = increase in bias

4.2. Conjugate gradient algorithms (CGAs)

Conjugate gradient algorithms (CGAs), one family of optimization methods, are considerably more efficient than GDAs, which have low memory consumption and provide quick convergence. Yet, it is occasionally unstable in large-scale issues [45]. CGAs are also useful for reducing functions with a large number of variables since no matrices must be stored [46]. The whole CGAs work by looking for the steepest descent direction [45], which is the inverse of the gradient provided in (2).

$$p_0 = -g_0 \tag{2}$$

Following that, a series calculation for a line search is performed as shown in (3) [47].

$$x_{k+1} = x_k + a_k p_k \tag{3}$$

The search direction is specified here with p_k. The next search direction is determined by (4) and is dependent on the prior search direction.

$$p_k = -g_k + \beta_k p_{k-1} - 1 \tag{4}$$

In CGAs, the calculation of constant k differs. Conjugate Gradient makes use of the Fletcher-Reeves (FR) update. Fletcher-Reeves Restarts (CGF) with Backpropagation Conjugate Gradient makes use of the Polak-Ribiére (PR) update. CGP Backpropagation with Polak/Ribiére Restarts [48]. The technique formulations are provided (5) and (6). Using computational methods PR outperforms FR in trials.

$$\beta_{k-1} = \left(\boldsymbol{g_k^T} + g_k\right)/\left(\boldsymbol{g_{k-1}^T} + g_{k-1}\right) \tag{5}$$

$$\beta_{k-1} = (g_k - g_{k-1})^T g_k / \left(\boldsymbol{g_{k-1}^T} + g_{k-1}\right) \tag{6}$$

In CGAs, the search direction is reset at regular intervals.

When the condition in (7) happens, the search direction in Conjugate Gradient with Powell/Beale Restarts (CGB) is reset to the negative of the gradient, increasing the training's efficiency [44].

$$|g_{k-1} * g_k| \geq 0.2 \|g_k\| \tag{7}$$

The last technique in this category is Scaled Conjugate Gradient Backpropagation (SCG), which leverages second order information from feedforward neural networks such as the Levenberg-Marquardt (LM) algorithm. It saves time by avoiding the time-consuming line searching at each iteration [43].

4.3. Gradient descent algorithms (GDAs)

BP algorithms learning provide the necessary and desired weights. Gradient descent backpropagation (GD), the batch steepest descent training technique, is the common BP algorithm that seeks to reduce network error as quickly as feasible. The GD algorithm defines one iteration as in (1). In GD, the weights are adjusted in proportion to a weight's error derivate's negative value. weight vector, and k denotes how many repetitions the procedures went through.

The simplest way to implement BP is via GD. Up until the network reaches a point of convergence, Eq. 8 is iterated.

$$x_{k+1} = x_k - a_k g_k \tag{8}$$

Quasi-Newton Algorithms (QNAs): QNAs are comparable to CGAs in terms of quick optimisation, and they may be viewed as the fundamental local approach utilising second-order information [49]. In comparison to CGAs, the algorithms' computational costs are higher, denser, and more sophisticated. Quasi-Newton (or secant) techniques are based on the Newton method but do not demand for the computation of second derivatives [50]. A gap between CGAs and QNAs is bridged using the one-step secant backpropagation (OSS) technique. OSS uses less storage and computations per epoch and does not retain the entire Hessian matrix.

4.4. Levenberg-marquardt algorithm (LM)

For the purpose of solving nonlinear least squares problems, LM is accepted as a standard approach. Combining the Gauss-Newton technique and gradient descent, it happens. When LM displays adaptive behaviour in response to the distance to the solution, it may frequently be certain of the answer [51]. The algorithm is sluggish and distant from the answer when BP is gradient descent [52]. On the other hand, if BP is Gauss-Newton, the method is very near to being accurate. For computing the gradient in LM, the estimated Hessian provided in (9) is computed in a slightly different way (10).

$$H = J^T J \tag{9}$$

$$g = JTe \tag{10}$$

where,

$\quad\quad J$ = Jacobian matrix

$\quad\quad e$ = vector of network errors

In conclusion, GDAs update the weights and biases in the direction of the performance function's negative gradient. CGAs look for the sharpest descending direction along conjugate directions, unlike GDAs. QNAs converge more quickly than CGAs and produce more accurate results. The computations might, however, take a while. Just the first derivative of the function is used in the conjugate gradient and the Quasi-Newton method. As higher derivatives are exceedingly expensive to calculate, these approaches are frequently favored in applications where only the first derivative is known.

5. Results

This section comprises discussions on the graphical representation of equipotential contours of typical days drawn with experimental data, followed by regression analysis for various algorithms and a comparative study of their performance in terms of speed vs. memory consumed.

5.1. Equi-potential contour for typical days

Fig. 6 shows the typical variation of the contour of HCP values on the 20th, 40th, 60th, 80th, 100th, 120th, 180th, 200th, 240th, and 270th days, respectively, for Slab #1. The contour plots provide a visual aid to perceive the variation in the HCP values with distance from the anode. The distance between consecutive contours indicates the rate of potential change. Closely spaced contour intervals indicate the poorer ability of concrete to resist chloride ions. The relatively regular intervals on the 20th day (Fig. 6a) show the migration of chloride ions towards the anode, with maxima at the centrally placed anode. Fig. 6(d) shows the equipotential contour plot on a typical rainy day. With very few circularly closely spaced contours near the anode, Fig. 6(h) indicates that most of the slab has a relatively constant potential, except near the anode. Thus, the consumption of chloride ions is evident, and the culmination of the experiment can be safely assumed. Localized contours in the remainder slab represent minor variations of the values in patches. Since the chloride ions were mixed with the mixing water while preparing the concrete, the HCP values throughout the testing period indicated a 90% corrosion possibility as per ASTM C876 [35].
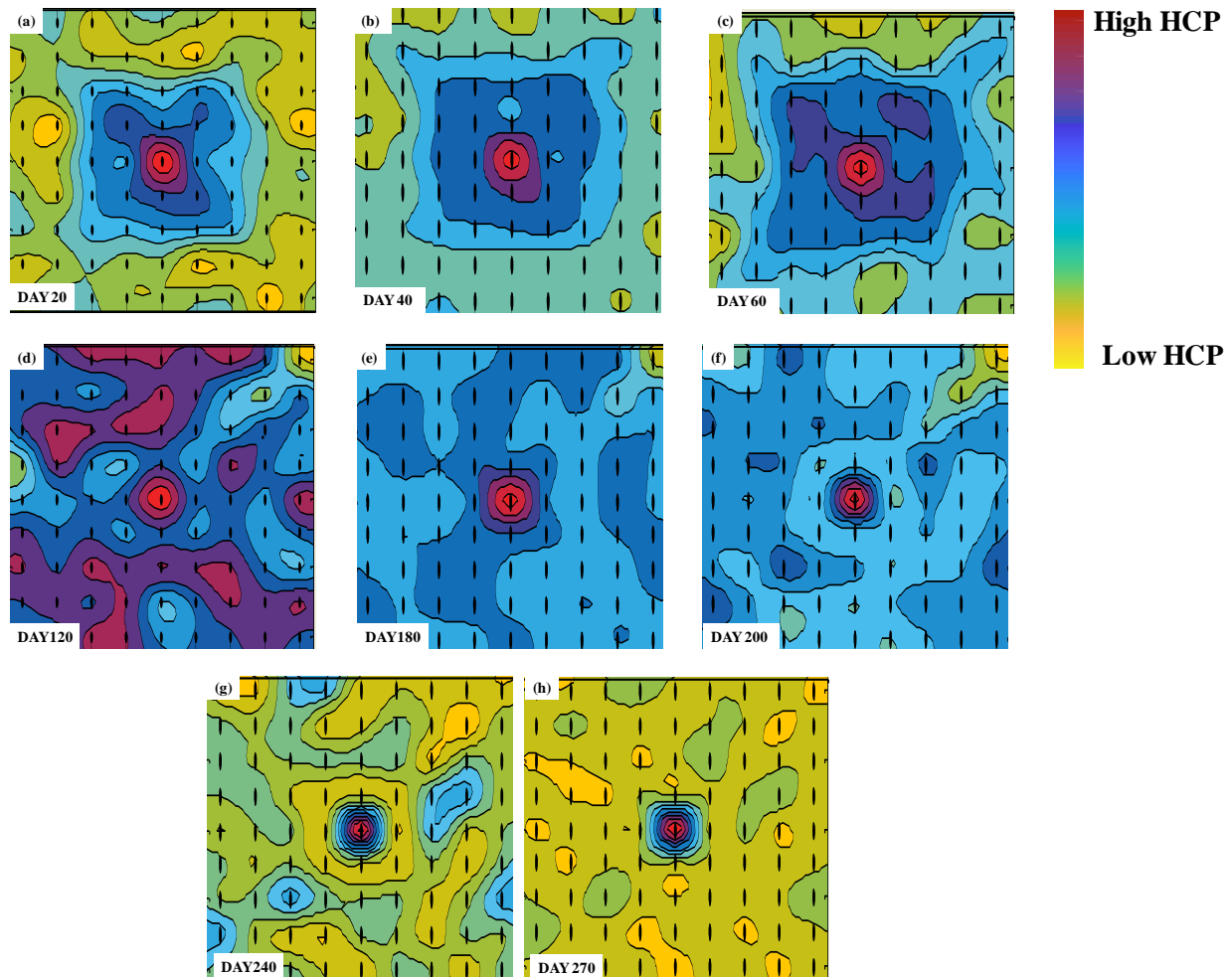

Fig. 6. (a-h) Equipotential contour plots for (a) 20th day, (b) 40th day, (c) 60th day, (d) 120th day, (e) 180th day, (f) 200th day, (g) 240th day, (h) 270th day.

The 3D representation of HCP values is shown in Fig. 7, with the z-axis representing the negative electrochemical potential values. A thin plate spline is used to map the 3D surface to obtain smooth interpolation between the set of control points. This enables a clearer visualisation of the gradual variation of HCP values along and across the anodes. The use of interpolant, cubic, and bi-harmonic transitions was hence avoided. The flattening of a relatively larger surface towards the 270th day (Fig. 7(h)) indicates the consumption of most of the chloride ions.
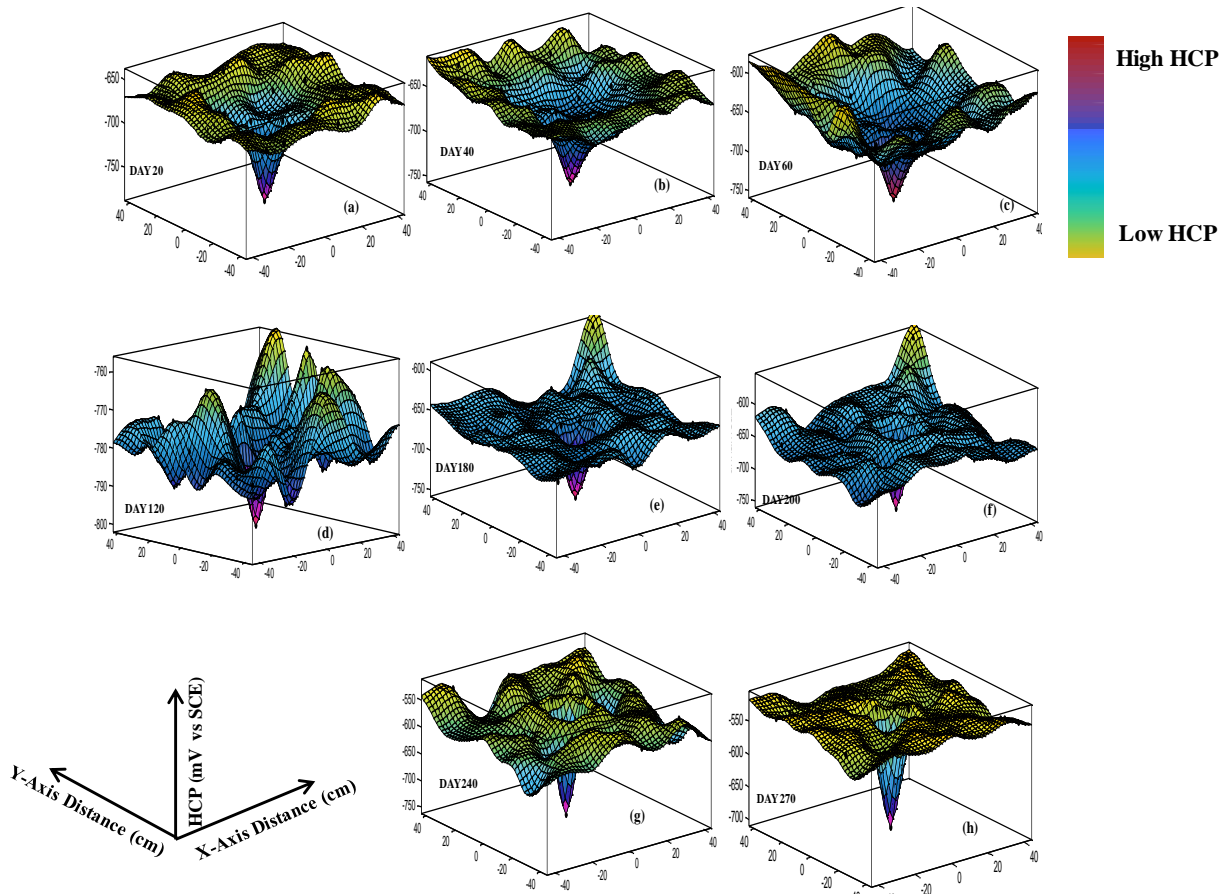

Fig. 7. (a-h) 3D equipotential contour plot for (a) 20th day, (b) 40th day, (c) 60th day, (d) 120th day, (e) 180th day, (f) 200th day, (g) 240th day, (h) 270th day.

5.2. Effect of distance, temperature, RH and age of concrete on potential

Several factors influence the HCP values and, hence, the corrosion probability of reinforcements in concrete slabs subjected to chloride ingress. These include chloride content, moisture content, compressive strength, clear cover, temperature, RH, distance from the anodes, and the age of the concrete. In this study, the inputs presented in previous literature, such as the age of the concrete, the distance from the anode, the temperature, and RH are considered. Other factors are kept constant throughout the experimental study.
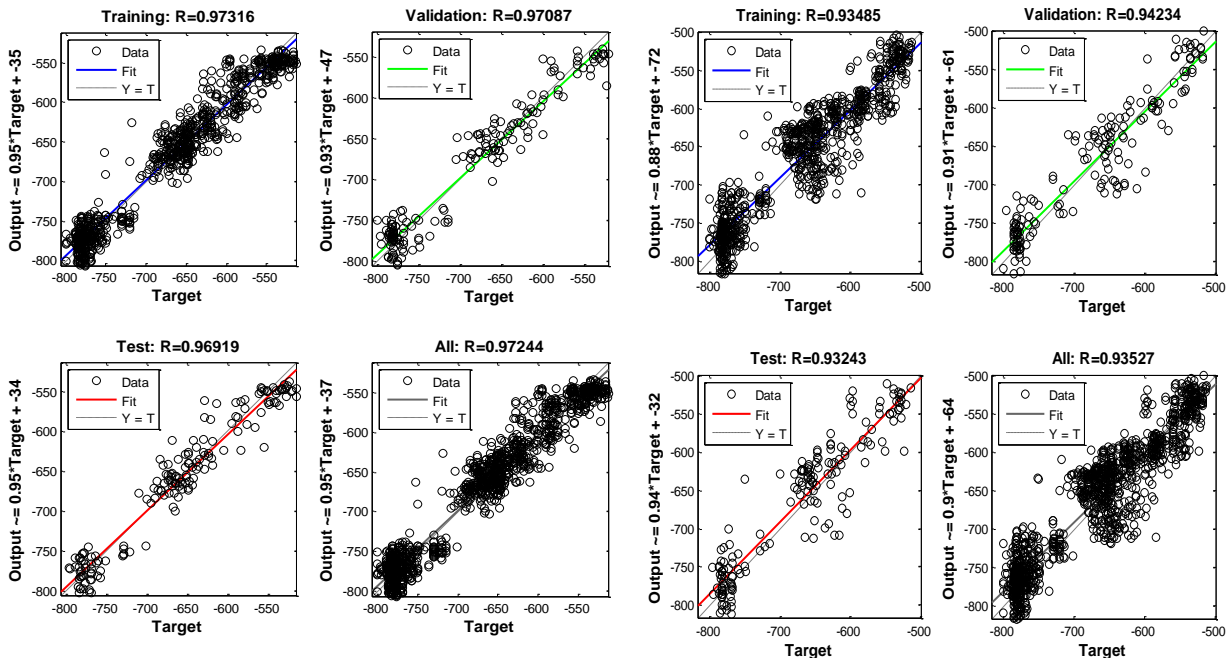
The result of regression analysis using feed-forward backpropagation with various algorithms is presented in Fig. 8. The ANN model was found exceptional in training, validation, and testing,

with an overall R greater than 96 percent for all cases. Thus, the model presented a clear relation between HCP values and environmental factors.
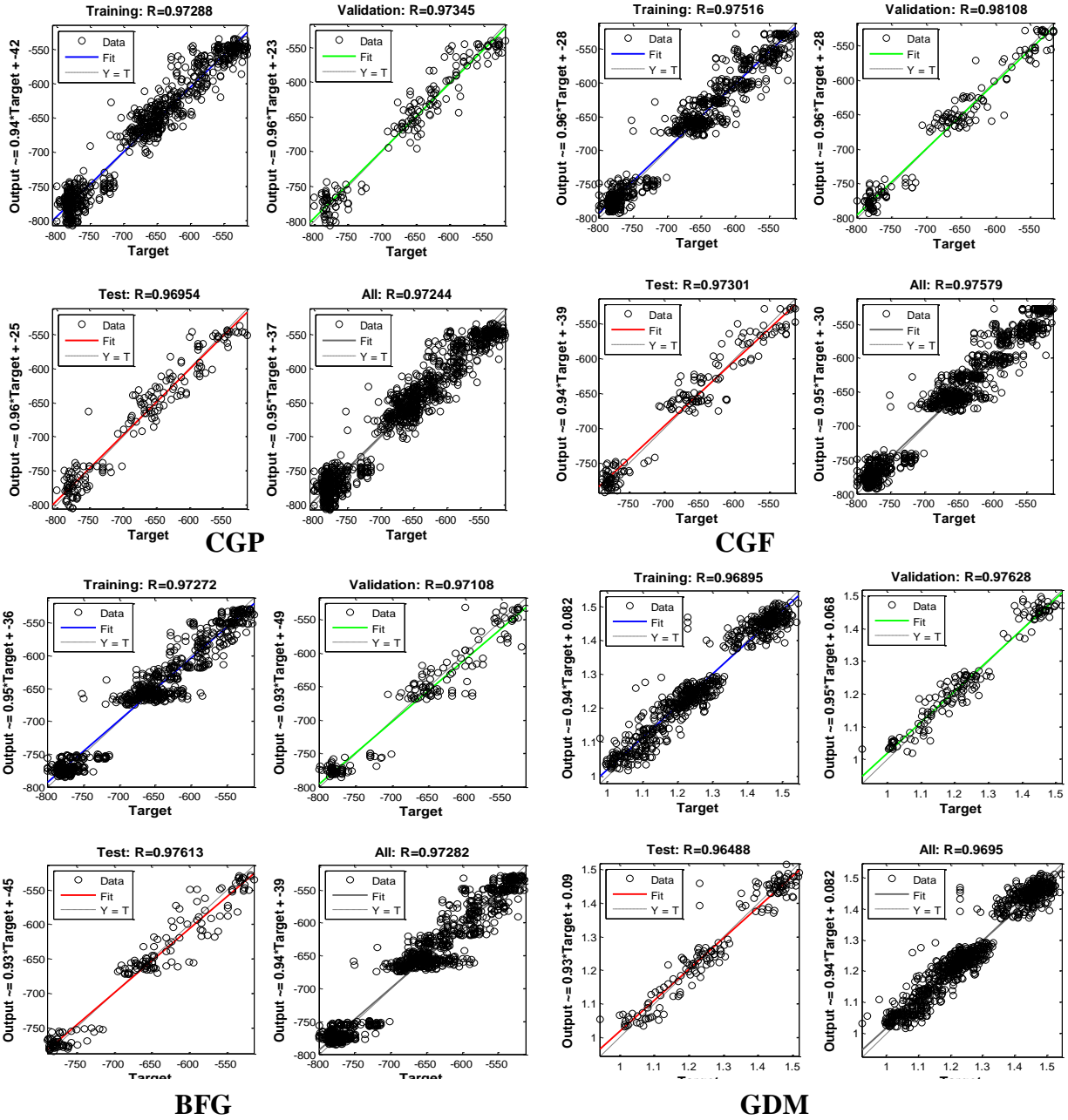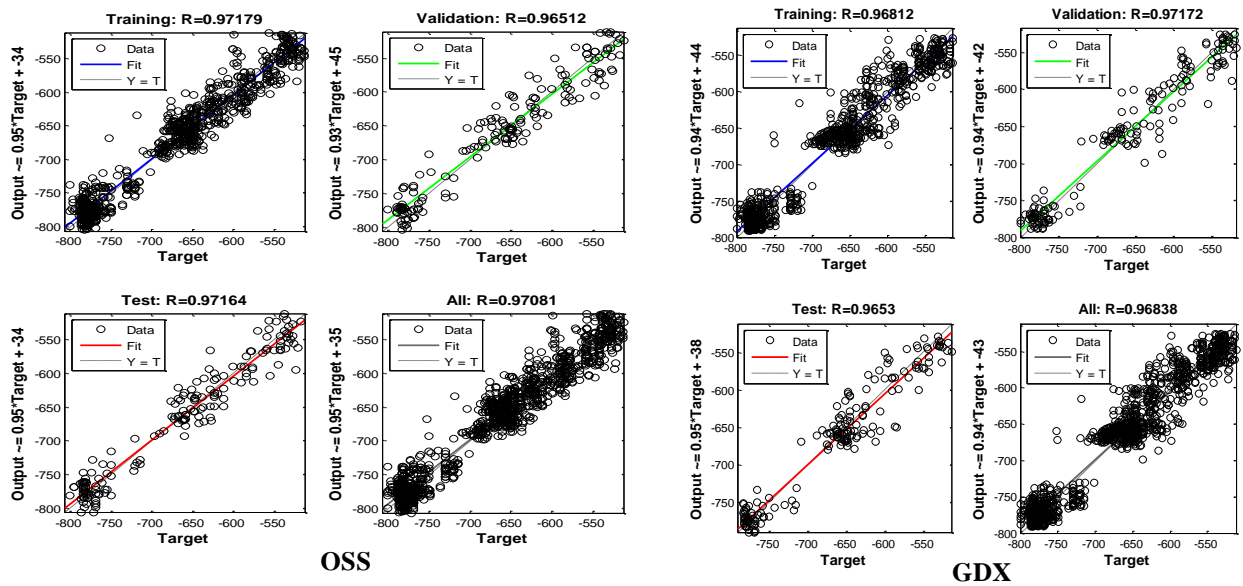

SCG

LMA

RB

GDA

CGP

CGF

BFG

GDM
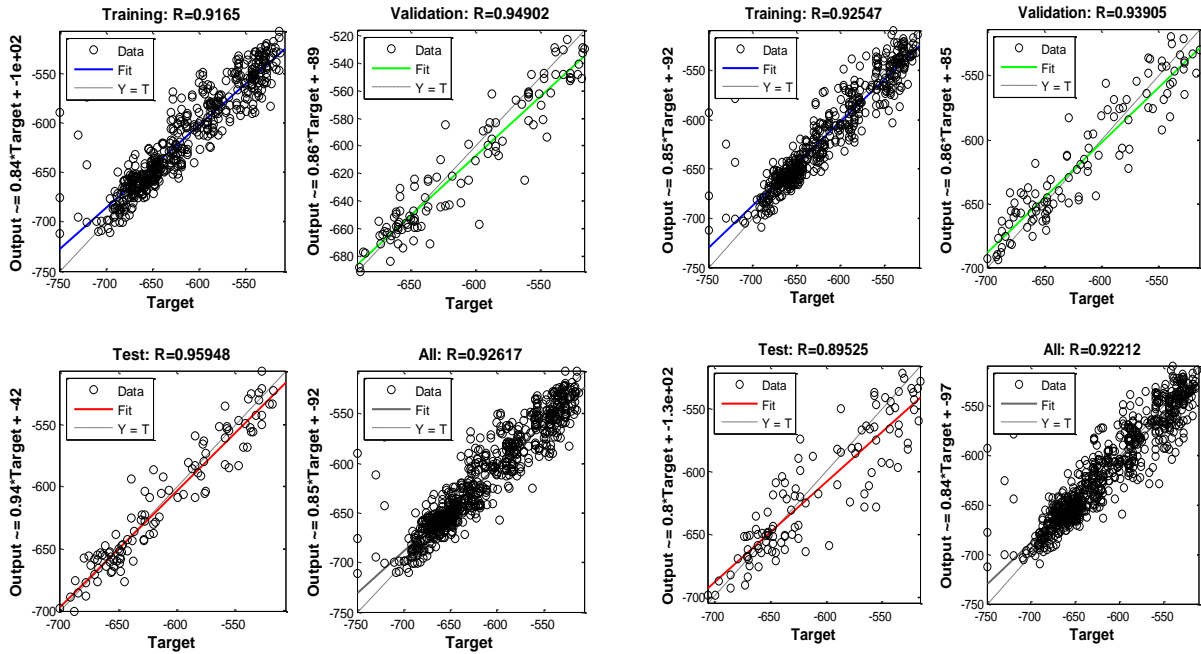
Fig. 8. Regression analysis using feed-forward backpropagation with various algorithms.

The graphical representation of predicted vs actual values of HCP is shown in Fig 9.
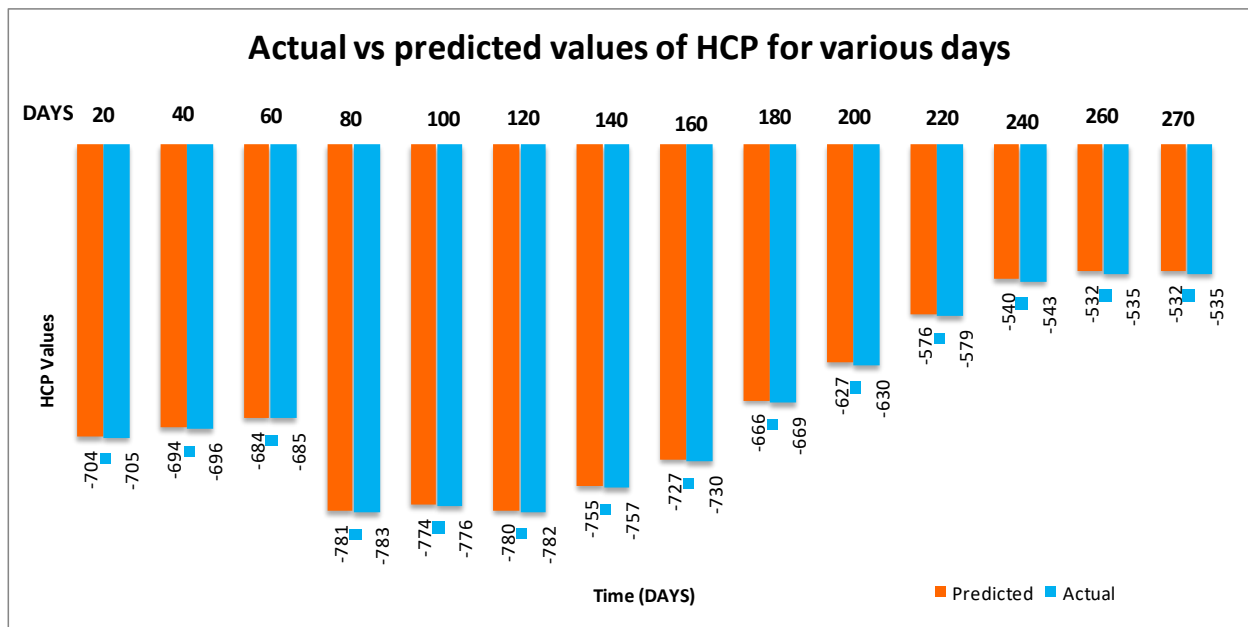

Fig. 9. Graphical representation of actual vs predicted values of HCP for various days.

5.3. Gradient error and epoch with different algorithms

Table 6 shows the variation of the gradient error and the corresponding epochs. For all of these algorithms, the number of validation checks is 6. The number of epochs initiated for training the algorithms was 500. From the table, it is evident that the lowest gradient error, is obtained in the case of LM at a considerably lower number of epochs of 28. The μ is obtained is maximum in the case of CGP, followed by GDA, GDX, CGF, OSS, SCG, RB, and LM.

Table 6
Variation of gradient error and epoch with different algorithms.

S. No.	Algorithm	Gradient Error (x 10^{-4})	Epoch
1	RB	2.01	95
2	OSS	2.84	58
3	SCG	2.33	59
4	GDA	40.7	86
5	CGP	79.8	6
6	CGF	30.0	59
7	GDX	36.7	141
8	LM	1.69	28

The number of epochs for various algorithms is also presented in Table 6. The maximum number of epochs is for GDX, followed by RB, GDA, SCG, and CGF, OSS, and LM, and the least number of epochs is that of CGP. It is seen that GDX involves the maximum number of epochs, of 141, and it also gives a substantial gradient error of 36.7 x 10^{-4}. With 6 epochs, CGP gives a maximum gradient error of 79.8 x 10^{-4}.

Hence, based on the above discussion, it can be inferred that the lowest gradient error is obtained with LM. Also, the number of epochs required by the LM algorithm to reach the minimum gradient error is just slightly more than the CGP. Thus, based on these results, it can be safely concluded that LM is the most accurate algorithm with significant speed to solve the present corrosion problem. Table 7 represents the statistical parameters used to evaluate the performance of all the algorithms along with the formula and criteria for evaluation. The parameters involved are Root Mean Square Error (RMSE), Coefficient of Variance (COV), Efficiency Coefficient (EC), Overall Index of Model Performance (OIMP) and Coefficient of Residual Mass (CRM).

RMSE has been utilized by researchers to compare predicted and observed parameters [53]. The RMSE numbers show how much the predictions underestimate or exceed the measurements. RMSE provides the advantage of stating the error using the identical units as the variable, offering additional information about the model's efficiency. The smaller the RMSE, the better is the forecast accuracy [54]. A value of 1.0 indicates a perfect match between measured and anticipated data, and this value might be negative.

Table 7
Algorithm performance evaluation in terms of statistical parameters.

| Statistical parameter	Formula	Desired Value	RB	OSS	SCG	GDA	CGP	CGF	GDX	LM
RMSE	$\sqrt{\dfrac{\sum_{i=1}^{n}(a_{p,i}-a_{0,i})^2}{n}}$	As less as possible	0.0333	0.321	0.0183	0.212	0.445	0.315	0.0165	0.0039
COV	$\dfrac{RMSE}{1/n\sum_{i=1}^{n}a_{0,i}}$ X 100	< 1.0	9.4055	9.0066	5.0993	4.123	12.623	5.012	2.015	1.0909
EC	$1-\dfrac{\sum_{i=1}^{n}(a_{p,i}-a_{0,i})^2}{\sum_{i=1}^{n}(a_{p,i}-a\prime_{0,i})^2}$	Larger the better, towards 1.0	0.9788	0.9803	0.9936	0.9745	0.7623	0.9541	0.9216	0.9997
OIMP	$\dfrac{1}{2}\left[1-\left(\dfrac{RMSE}{a_{max}-a_{min}}\right)+EC\right]$	Larger the better	0.9719	0.9733	0.9872	0.9717	0.8578	0.9318	0.9127	0.9978
CRM	$\dfrac{\left(\sum_{i=1}^{n}a_{p,i}-\sum_{i=1}^{n}a_{0,i}\right)}{\sum_{i=1}^{n}a_{0,i}}$	As close to zero as possible	-0.0016	0.0050	0.0086	0.0081	-0.0670	0.0078	0.0084	-0.009
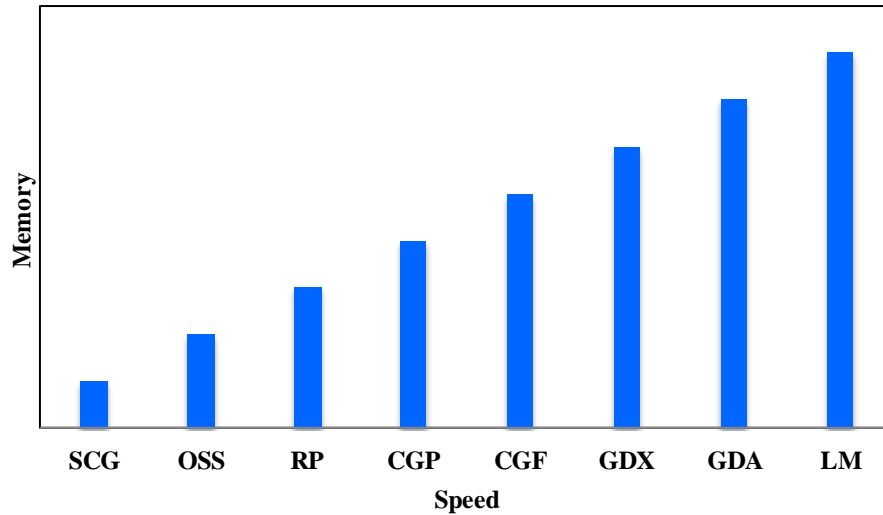
Fig. 10. Performance comparison of various algorithms in terms of memory and speed.

The EC value might be positive or negative, with 1.0 denoting a perfect match between the observed and anticipated data. OIMP was used to test the effectiveness of mathematical models. A model with an OIMP value of 1 has a perfect match between the measured and projected values [55]. The CRM parameter displays the difference between measured and forecasted values in comparison to the measured data. The CRM is used to assess the model's propensity to exaggerate or underestimate measured data. A zero value indicates a perfect match, but positive and negative values show the model's under- and over-prediction, respectively. The optimal training algorithm was chosen based on the lowest RMSE and CRM, as well as the greatest EC and OIMP values. From Table 7, and based on the above discussion, it is seen that for the prediction of HCP values the RMSE and CRM values are very near to zero and the values of EC, COV and OIMP are approximately equal to one in the case of LM. Hence, in terms of statistical performance, the LM algorithm can be concluded to be the best. Further the statistical performance of CGP was found to be the least. A graphical representation of performance of various algorithms in terms of memory and speed is shown in Fig. 10. It is seen that LM requires maximum memory and has highest speed.

6. Conclusions

Based on the experimental data collected for 80 points each for 270 days on two sets of slabs, several ANN algorithms were studied to predict the variation in HCP values of an RCC slab containing pure Mg sacrificial anodes subjected to chloride ingress. The distance of the point under consideration from the anode in x and y-axis, temperature, RH and age of concrete in days were considered as input parameters. From the several trials, a two-layer feed-forward network with sigmoid hidden neurons and linear output neurons trained with Levenberg-Marquardt backpropagation with network architectures [5-10-1] was chosen as the best structure. The effect of varying training and validation percentages was also studied. It is concluded that the regression coefficients were significantly comparable for all ratios of training and validation. The prediction of HCP values through a neural network model based on the available experimental

data set is excellent. Further, from the results, it is found that slab #1 corresponds to a slab with 90% probability of corrosion (as 3.5% NaCl is mixed with the concrete while it is being cast), while slab #2 exits in the zone of 90% probability of no corrosion, according to ASTM C-876. These models can be used to predict the future values of HCP and, hence, the possibility of corrosion of the embedded reinforcements. Models can also be developed to predict the presence of free chloride ions, given the HCP value. This will enable the prediction of potential corrosion sites in the RCC slabs. Based on statistical parameters the performance of LM method was found to be the best. The present work considered sigmoid type of activation function. However, the type of activation functions plays a major role in the accuracy of ANN models and the performance of these algorithms with different types of activation functions could be considered in future. It is also suggested to develop HCP prediction models for early and long curing data.

Acknowledgement

Funding

Conflict of interest

The authors declare that they have no conflict of interest.

Data availability statement

The data that support the findings of this study are available from the corresponding author upon reasonable request

Contributions of author

Conceptualization; Data curation; Formal analysis; Software; Validation; Visualization; Writing - original draft; Writing - review & editing.

References

[1]   Karni J. The durability of prefabricated reinforced concrete external walls and cladding in buildings. Durab. Build. Mater. components. Second Int. Conf. Gaithesbg., 1981, p. 188–93.

[2]   Fu HC, Erki MA, Seckin M. Review of Effects of Loading Rate on Reinforced Concrete. J Struct Eng 1991;117:3660–79. https://doi.org/10.1061/(asce)0733-9445(1991)117:12(3660).

[3]   Kumar V. Protection of Steel Reinforcement. Corros Rev 1998;002:317–58.

[4]   Islam, S. S., Islam, M. N., & Sobhan MA. Corrosion of Reinforced Concrete Structures Exposed to Marine Environment: A Review. Ournal Civ Eng Archit 2016;10:663-674.

[5]   Fadayomi J. Corrosion inhibitors. Concr 1997;31:21–2.

[6]   Söylev TA, Richardson MG. Corrosion inhibitors for steel in concrete: State-of-the-art report. Constr Build Mater 2008. https://doi.org/10.1016/j.conbuildmat.2006.10.013.

[7]   Ormellese M, Berra M, Bolzoni F, Pastore T. Corrosion inhibitors for chlorides induced corrosion in reinforced concrete structures. Cem Concr Res 2006;36:536–47. https://doi.org/10.1016/j.cemconres.2005.11.007.

[8]   Elsener B, Angst U. Corrosion inhibitors for reinforced concrete. Sci. Technol. Concr. Admixtures, 2016. https://doi.org/10.1016/B978-0-08-100693-1.00014-X.

[9]   Al-Sodani KAA, Al-Amoudi OSB, Maslehuddin M, Shameem M. Efficiency of corrosion inhibitors in mitigating corrosion of steel under elevated temperature and chloride concentration. Constr Build Mater 2018;163:97–112. https://doi.org/10.1016/j.conbuildmat.2017.12.097.

[10] Dias P, Carneiro C, Andrade L, Sousa J, Machado J, Mendes A. Characterization of a water-based paint for corrosion protection. J Coatings Technol Res 2012. https://doi.org/10.1007/s11998-011-9388-0.

[11] Dong S, Zhao B, Lin C, Du R, Hu R, Zhang GX. Corrosion behavior of epoxy/zinc duplex coated rebar embedded in concrete in ocean environment. Constr Build Mater 2012. https://doi.org/10.1016/j.conbuildmat.2011.08.026.

[12] Ahmad Z, Al-Sulaiman F, Abdul Aleem BJ. Corrosion behavior of carbon reinforced plain-weave laminates. J Reinf Plast Compos 2004. https://doi.org/10.1177/0731684404035268.

[13] Bertolini L, Carsana M, Gastaldi M, Lollini F, Redaelli E. Corrosion of steel in concrete and its prevention in aggressive chloride-bearing environments. Int Conf Durab Concr Struct ICDCS 2016 2016:13–25. https://doi.org/10.5703/1288284316106.

[14] Parthiban GT, Parthiban T, Ravi R, Saraswathy V, Palaniswamy N, Sivan V. Cathodic protection of steel in concrete using magnesium alloy anode. Corros Sci 2008;50:3329–35. https://doi.org/10.1016/j.corsci.2008.08.040.

[15] Leeds S, Leeds J. Cathodic Protection. Oil Gas Pipelines Integr. Saf. Handb., 2015. https://doi.org/10.1002/9781119019213.ch32.

[16] Szabó S, Bakos I. Cathodic protection with sacrificial anodes. Corros Rev 2006. https://doi.org/10.1515/CORRREV.2006.24.3-4.231.

[17] Murthy YI, Gandhi S, Kumar A. Corrosion Prevention of Steel Reinforcement in 7.5% NaCl Solution using Pure Magnesium Anode. IOP Conf. Ser. Mater. Sci. Eng., 2018. https://doi.org/10.1088/1757-899X/330/1/012003.

[18] Murthy YI, Gandhi S, Kumar A. Magnesium alloy anodes for corrosion prevention of reinforcements in concrete. Int J Emerg Technol 2020.

[19] Andrei M, Di Gabriele F, Bonora PL, Scantlebury D. Corrosion behaviour of magnesium sacrificial anodes in tap water. Mater Corros 2003. https://doi.org/10.1002/maco.200390010.

[20] Rousseau C, Baraud F, Leleyter L, Gil O. Cathodic protection by zinc sacrificial anodes: Impact on marine sediment metallic contamination. J Hazard Mater 2009. https://doi.org/10.1016/j.jhazmat.2009.01.083.

[21] WANG N, WANG R, PENG C, HU C, FENG Y, PENG B. Research progress of magnesium anodes and their applications in chemical power sources. Trans Nonferrous Met Soc China 2014;24:2427–39. https://doi.org/10.1016/S1003-6326(14)63367-7.

[22] Cheung MMS, Cao C. Application of cathodic protection for controlling macrocell corrosion in chloride contaminated RC structures. Constr Build Mater 2013. https://doi.org/10.1016/j.conbuildmat.2013.04.010.

[23] Liu G, Zhang Y, Ni Z, Huang R. Corrosion behavior of steel submitted to chloride and sulphate ions in simulated concrete pore solution. Constr Build Mater 2016;115:1–5. https://doi.org/10.1016/j.conbuildmat.2016.03.213.

[24] Nissi Joy C, Ramakrishnan K, Snega M, Ramasundram S, Venkatasubramanian C, Muthu D. Study on Strength and Durability Characteristics of Concrete with Ternary Blend. IOP Conf Ser Earth Environ Sci 2017;80:012022. https://doi.org/10.1088/1755-1315/80/1/012022.

[25] Macdonald DD, Miller TA. Cathodic Protection of Reinforced Concrete Structures: A Review. Corros Rev, 1994;12:73–96. https://doi.org/10.1515/CORRREV.1994.12.1-2.73.

[26] Tang D, Du Y, Li X, Liang Y, Lu M. Effect of alternating current on the performance of magnesium sacrificial anode. Mater Des 2016;93:133–45. https://doi.org/10.1016/j.matdes.2015.12.112.

[27] Yu B, Yang L, Wu M, Li B. Practical model for predicting corrosion rate of steel reinforcement in concrete structures. Constr Build Mater 2014;54:385–401. https://doi.org/10.1016/j.conbuildmat.2013.12.046.

[28] Ouzaa K, Oucif C. Numerical model for prediction of corrosion of steel reinforcements in reinforced concrete structures. Undergr Sp 2019;4:72–7. https://doi.org/10.1016/j.undsp.2018.06.002.

[29] Hodhod OA, Ahmed HI. Modeling the corrosion initiation time of slag concrete using the artificial neural network. HBRC J 2014;10:231–4. https://doi.org/10.1016/j.hbrcj.2013.12.002.

[30] Thike PH, Zhao Z, Shi P, Jin Y. Significance of artificial neural network analytical models in materials' performance prediction. Bull Mater Sci 2020;43. https://doi.org/10.1007/s12034-020-02154-y.

[31] Roxas CLC, Lejano BA. An artificial neural network model for the corrosion current density of steel in mortar mixed with seawater. Int J GEOMATE 2019;16:79–84. https://doi.org/10.21660/2019.56.4585.

[32] Taffese WZ. Data-Driven Method for Enhanced Corrosion Assessment of Reinforced Concrete Structures 2020.

[33] Elsener B. Half-cell potential mapping to assess repair work on RC structures. Constr Build Mater 2001. https://doi.org/10.1016/S0950-0618(00)00062-3.

[34] ASTM International. Standard test method for corrosion potentials of uncoated reinforcing steel in concrete. ASTM C876 - 15. G01.14,. ASTM Int 2015.

[35] Bureau of Indian Standards, "IS:456-2000," Plain and Reinforced Concrete - Code of Practice , Reaffirmed 2021 n.d.

[36] BIS: 10262-2019 ''Recommended guidelines for concrete mix design." Bureau, of Indian Standards, New Delhi I. No Title n.d.

[37] IS:12269-2013. ORDINARY PORTLAND CEMENT , 53 grade specification (First Revision). Bur Indian Stand New Delhi, India 2013.

[38] (Bureau of Indian Standards ND. IS : 383-2016. Indian Stand Specif Coarse Fine Aggregates from Nat Sources Concr Third Revis Reaffirmed 2016 n.d.

[39] McCulloch W, Pitts W. A Logical Calculus of the Ideas Immanent in Nervous Activity (1943). Ideas That Creat. Futur., vol. 5, The MIT Press; 2021, p. 79–88. https://doi.org/10.7551/mitpress/12274.003.0011.

[40] Basheer, I. A., & Hajmeer M. Artificial neural networks: fundamentals, computing, design, and application. J Microbiol Methods 2000;43:3-31.

[41] Pomplun M, Jone AAA, Sagayam KM, Xavier KA, Narmadha D, Sundar GN, et al. Intelligent computational techniques of machine learning models for demand analysis and prediction. Int J Intell Inf Database Syst 2022;1:1. https://doi.org/10.1504/IJIIDS.2022.10051510.

[42]   Skare EL, Sheiati S, Cepuritis R, Mørtsell E, Smeplass S, Spangenberg J, et al. Rheology modelling of cement paste with manufactured sand and silica fume: Comparing suspension models with artificial neural network predictions. Constr Build Mater 2022;317:126114. https://doi.org/10.1016/j.conbuildmat.2021.126114.

[43]   Sheiati S, Ranjbar N, Frellsen J, Skare EL, Cepuritis R, Jacobsen S, et al. Neural network predictions of the simulated rheological response of cement paste in the FlowCyl. Neural Comput Appl 2021;33:13027–37. https://doi.org/10.1007/s00521-021-05999-4.

[44]   Riedmiller M, Braun H. A direct adaptive method for faster backpropagation learning: the RPROP algorithm. IEEE Int. Conf. Neural Networks, IEEE; n.d., p. 586–91. https://doi.org/10.1109/ICNN.1993.298623.

[45]   Mller AJ, Call JE, Whiting RC. Comparison of Organic Acid Salts for Clostridium botulinum Control in an Uncured Turkey Product. J Food Prot 1993;56:958–62. https://doi.org/10.4315/0362-028X-56.11.958.

[46]   MJ. P. Restart procedures for the conjugate gradient method. Math Program 1977;12:241-54.

[47]   Lucas RJ, Peirson SN, Berson DM, Brown TM, Cooper HM, Czeisler CA, Figueiro MG, Gamlin PD, Lockley SW, O'Hagan JB PL. Measuring and using light in the melanopsin age. Trends Neurosci 2014;37:1–14.

[48]   El-Nabarawy I, Abdelbar AM WD. Levenberg-Marquardt and Conjugate Gradient methods applied to a high-order neural network. Int. Jt. Conf. neural networks, 2013, p. 1–7.

[49]   Battiti R. First-and second-order methods for learning: between steepest descent and Newton's method. Neural Comput 1992;4:141-66.

[50]   Dennis JE, Schnabel RB. Numerical Methods for Unconstrained Optimization and Nonlinear Equations. vol. 242. Society for Industrial and Applied Mathematics; 1996. https://doi.org/10.1137/1.9781611971200.

[51]   Marquardt DW. An Algorithm for Least-Squares Estimation of Nonlinear Parameters. J Soc Ind Appl Math 1963;11:431–41. https://doi.org/10.1137/0111030.

[52]   Hagan MT, Menhaj MB. Training Feedforward Networks with the Marquardt Algorithm. IEEE Trans Neural Networks 1994;5:989–93. https://doi.org/10.1109/72.329697.

[53]   Arbat G, Puig-Bargués J, Barragán J, Bonany J, Ramírez de Cartagena F. Monitoring soil water status for micro-irrigation management versus modelling approach. Biosyst Eng 2008;100:286–96. https://doi.org/10.1016/j.biosystemseng.2008.02.008.

[54]   Legates DR, McCabe GJ. Evaluating the use of "goodness-of-fit" measures in hydrologic and hydroclimatic model validation. Water Resour Res 1999;35:233–41. https://doi.org/10.1029/1998WR900018.

[55]   Alazba AA, Mattar MA, ElNesr MN, Amin MT. Field Assessment of Friction Head Loss and Friction Correction Factor Equations. J Irrig Drain Eng 2012;138:166–76. https://doi.org/10.1061/(asce)ir.1943-4774.0000387.